Magnon blockade based on the Kerr nonlinearity in cavity electromagnonics

Rui Hou,[1] Wei Zhang,[2] Xue Han,[1,*] Hong-Fu Wang,[1,†] and Shou Zhang[1,‡]
[1]*Department of Physics, College of Science, Yanbian University, Yanji, Jilin 133002, China*
[2]*School of Physics, Harbin Institute of Technology, Harbin, Heilongjiang 150001, China*

(Received 15 December 2023; accepted 12 March 2024; published 22 March 2024)

Magnon blockade is an effective physical mechanism to generate a single magnon, which is of great importance in quantum information processing. We present a scheme to realize the unconventional magnon blockade effect by using Kerr nonlinearity in a cavity electromagnonic system. Under weak driving conditions, we give the optimal parameter conditions for magnon antibunching through analytical calculations, which are in good agreement with numerical results. Furthermore, we find that Kerr nonlinearity is necessary to create magnon blockade. In particular, unconventional magnon blockade can be achieved in both weak nonlinearity and weak coupling regimes. The present scheme indicates a method for generating unconventional magnon blockade effect and provides a feasible and flexible platform for the realization of a single-magnon source with high purity.

DOI: 10.1103/PhysRevA.109.033721

I. INTRODUCTION

Hybrid quantum systems that combine the advantages of different quantum subsystems play an important role in the fields of quantum technology, quantum information processing, and quantum sensing [1–3]. In recent years, hybrid quantum systems based on collective spin excitations in ferromagnetic crystals have developed rapidly [4–12]. A variety of quantum phenomena, including magnon-photon-phonon entanglement [13–15], mechanical squeezing [16,17], as well as photon and magnon blockade (MB) [18–24], have been extensively investigated both theoretically and experimentally. Cavity electromagnonics serves as the basis of almost all hybrid systems based on magnonics, focusing on the interaction between magnetic spin waves [25] and microwave photons. A typical cavity electromagnonic system consists of the microwave cavity and yttrium iron garnet (YIG), which serves as a highly desirable ferromagnetic material due to its high spin density and low dissipation rate [26–28]. The hybrid quantum system containing magnons is different from the conventional cavity optomechanical system [29,30]. By utilizing the magnetic dipole interaction, the coupling between magnons and microwave photons can be achieved.

The MB effect, similar to the photon blockade effect [31], implies that the absorption of the first few magnons will block the transmission of subsequent magnons. The MB effect is divided into conventional magnon blockade (CMB) and unconventional magnon blockade (UMB) due to different physical mechanisms. The CMB effect is caused by the anharmonicity of the energy spectrum in the system, while the UMB effect is induced by the destructive quantum interference between different transition paths. The MB effect in a hybrid ferromagnet-superconductor quantum system was first proposed in 2019 [18], subsequently demonstrated in a hybrid quantum system of a three-dimensional microwave cavity coupled to both a small YIG sphere and a superconducting qubit [21], and explored in a hybrid ferromagnet-superconductor system with two qubits [32]. Recently, the simultaneous photon-phonon-magnon blockade has been achieved in a hybrid microwave optomechanical-magnetic system [33]. Meanwhile, the MB effect has been extended to the multimagnon regime, which has been studied in a hybrid superconducting system [34].

As a nonlinear interaction between fields and waves, the Kerr interaction [35–38] can be employed for the realization of quantum logic gates [39,40] and the generation of entangled photons [41,42]. The photon blockade effect has been studied using the cross-Kerr interaction between the cavity and mechanical modes [43,44] as well as two resonators [45]. Also, a scheme has been proposed to implement the unconventional photon blockade effect via the cavity self-Kerr coupling and the intercavity cross-Kerr coupling in a four-mode optomechanical system [46]. Recently, a scheme has been proposed to investigate the MB effect in cavity magnon systems by utilizing cross-Kerr interactions between cavity modes [23,47]. However, this scheme uses the Heisenberg equation of motion to consider the dynamics of the system. Therefore, an intriguing question arises here: is it possible to study the MB effect using the master equation to describe the dynamic evolution of the system?

Inspired by the above-mentioned works, in this paper, we present an efficient method for realizing UMB in both strong-coupling and weak-coupling regimes. Here, strong coupling [48,49] (weak coupling) means that the magnon-photon coupling strength is larger (less) than the decay rate of the modes. The magnon-photon coupling strength can be changed by adjusting the position of the YIG sphere. We study the MB effect based on Kerr nonlinearity in the cavity electromagnonic system, by analytically and numerically calculating

*xuehan@ybu.edu.cn
†hfwang@ybu.edu.cn
‡szhang@ybu.edu.cn

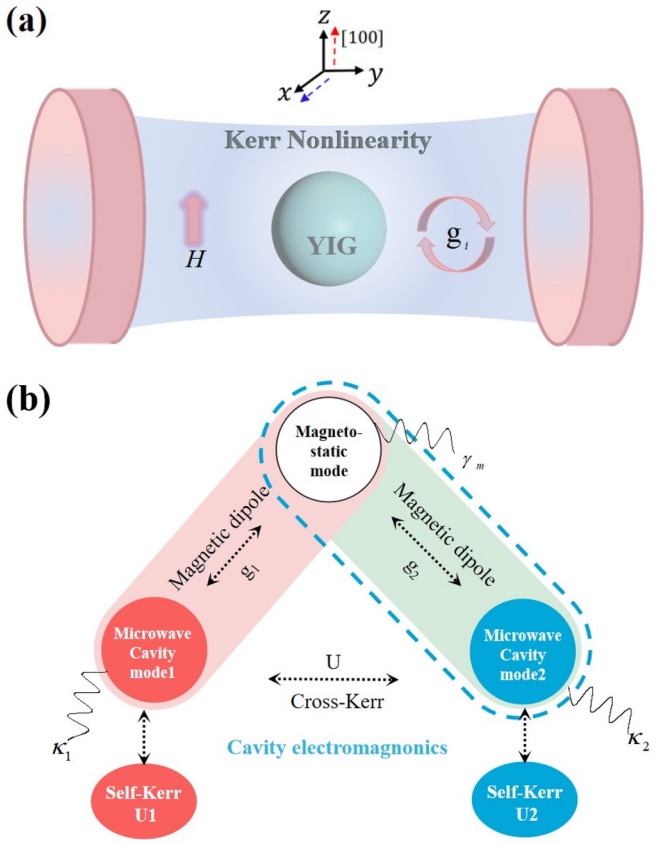

FIG. 1. (a) Schematic diagram of the cavity electromagnonic system consisting of two microwave cavity modes in an optical cavity within a Kerr medium and a magnon mode. (b) Diagram of a magnon mode interacting with two microwave cavity modes in a microwave cavity containing Kerr medium.

the equal-time second-order correlation function of magnons using wave function and density matrix methods, respectively. We find that the numerical results agree with the analytical calculations. In particular, Kerr nonlinearity is necessary to achieve magnon antibunching. This work may provide an experimentally implementable method for the observation of the MB effect in the cavity electromagnonic system.

This paper is organized as follows. In Sec. II, we derive the Hamiltonian of the cavity electromagnonic system consisting of two microwave cavity modes and a magnon mode. In Sec. III, we analytically and numerically solve the equal-time second-order correlation functions and give the optimal parameter conditions for UMB. In Sec. IV, we discuss the influence of tunable parameters on the UMB. Finally, a conclusion is given in Sec. V.

II. SYSTEM MODEL

We consider a cavity electromagnonic system in which a two-mode quantized radiation field (with specific standing wave field distributions) oscillating in frequencies ω_1 and ω_2 interacts with the magnon mode (with frequency ω_m) in a YIG sphere in a microwave cavity containing Kerr medium, as depicted in Fig. 1. Using this centrosymmetric nonlinear medium, both self-Kerr and cross-Kerr nonlinearities are considered simultaneously in the system. The magnons are embodied by the collective excitation of a large number of spins inside a YIG sphere. The YIG sphere (250 μm diameter) is mounted at the antinode of the magnetic field of the cavity mode and magnetized to saturation by a bias magnetic field H. The bias magnetic field (z direction), the magnetic field (x direction) of the microwave cavity mode, and the drive field magnetic component (y direction) are perpendicular to each other at the position of the YIG sphere. This maximizes the strength of the magnon-photon coupling. The magnon mode is directly driven by a microwave source with frequency ω_d. In a frame rotating at the driving frequency ω_d, the total Hamiltonian of the system is written as ($\hbar = 1$)

$$H = H_0 + H_I + H_k + H_d. \tag{1}$$

H_0 corresponds to the free Hamiltonian of two microwave cavity modes and a magnon mode, which can be given by

$$H_0 = \Delta_1 a_1^\dagger a_1 + \Delta_2 a_2^\dagger a_2 + \Delta_m m^\dagger m, \tag{2}$$

where $a_i^\dagger(a_i)$ and $m^\dagger(m)$ are the creation (annihilation) operators of the microwave cavity and magnon modes, respectively. For clarity, Table I concludes the definitions of operators, frequencies, and decay rates for the physical systems considered in this paper. Here, $\Delta_{(i,m)} = \omega_{(i,,m)} - \omega_d$ is the driving detuning. H_I represents the interaction between microwave cavity modes and the magnon mode. The Hamiltonian can be described by

$$H_I = g_1(a_1^\dagger m + a_1 m^\dagger) + g_2(a_2^\dagger m + a_2 m^\dagger), \tag{3}$$

where g_i is the magnon-photon coupling strength. The magnetic dipole interaction mediates the coupling between magnons and microwave photons. H_k refers to the self-Kerr and cross-Kerr nonlinearity of microwave cavity modes. It reads as

$$H_k = -U_1 a_1^\dagger a_1 a_1^\dagger a_1 - U_2 a_2^\dagger a_2 a_2^\dagger a_2 - U a_1^\dagger a_1 a_2^\dagger a_2, \tag{4}$$

where $U_i = 3(\hbar\omega_i)^2\bar{\chi}^{(3)}/(4\varepsilon_0 V_{\text{eff}}\bar{\varepsilon}_r^2)$ is the self-Kerr nonlinear coefficient of the microwave cavity mode. To have order-of-magnitude results, we assume constant values for the average real part of the nonlinear susceptibility and relative dielectric permittivity, $\bar{\chi}^{(3)}$ and $\bar{\varepsilon}_r^2$, respectively. ε_0 is the vacuum permittivity, and V_{eff} is the effective mode volume. U is the cross-Kerr coefficient between the two microwave cavity modes. Meanwhile, the self-Kerr and cross-Kerr coefficients satisfy the following relationship: $U_1 = U_2 = U/2$ [50]. H_d denotes the magnon mode is directly driven by a microwave source. It is given by

$$H_d = \Omega_d(m^\dagger + m). \tag{5}$$

The Rabi frequency $\Omega_d = (\sqrt{5}/4)\gamma_0\sqrt{N}B_0$ denotes the coupling strength between the magnon mode and its driving magnetic field with amplitude B_0 and frequency ω_d, where γ_0 is the gyromagnetic ratio, and the total number of spins $N = \rho V$ with the spin density ρ and the volume of the sphere V. The experimentally accessible parameters are chosen as [13,51,52] $\omega_i/2\pi = 10$ GHz, $\omega_m/2\pi = 10$ GHz, $\kappa_i/2\pi = 1$ MHz, $\gamma_m/2\pi = 1$ MHz, $V_{\text{eff}} = 0.01\,\mu\text{m}^3$, $\bar{\chi}^{(3)}/\bar{\varepsilon}_r^2 = 2\times10^{-17}\,\text{m}^2/\text{V}^2$, $\gamma_0/2\pi = 28$ GHz/T, and $\rho = 4.22\times10^{27}\,\text{m}^{-3}$.

TABLE I. Bosonic operators, and typical values for the frequencies and decay rates of the modes of the different physical systems.

Physical system	Mode	Operators	Frequency	Decay rate
Microwave cavity	Microwave cavity mode i ($i = 1, 2$)	$\hat{a}_i, \hat{a}_i^\dagger$	$\omega_i/2\pi \sim 10$ GHz	$\kappa_i/2\pi \sim 1$ MHz
Ferromagnetic crystal	Magnetostatic mode	$\hat{m}, \hat{m}^\dagger$	$\omega_m/2\pi \sim 10$ GHz	$\gamma_m/2\pi \sim 1$ MHz

III. MAGNON STATISTICAL PROPERTIES

The statistic properties of the magnon will be described by the equal-time second-order correlation function in the steady state, which can be obtained through analytically solving the non-Hermitian Schrödinger equation and numerically simulating the quantum master equation.

A. Analytical solution

Here, the non-Hermitian Hamiltonian is given by adding phenomenologically the decay rate

$$H_{\rm non} = H - \frac{i\kappa_1}{2}a_1^\dagger a_1 - \frac{i\kappa_2}{2}a_2^\dagger a_2 - \frac{i\gamma_m}{2}m^\dagger m. \tag{6}$$

Under the weak driving condition ($\Omega_d \ll \gamma_m$), the Hilbert space of the system can be limited in the low-excitation subspace (up to 2). Therefore, the wave function for the system can be expressed as

$$\begin{aligned}|\psi\rangle = {} & C_{000}|000\rangle + C_{001}|001\rangle + C_{100}|100\rangle \\ & + C_{010}|010\rangle + C_{002}|002\rangle + C_{101}|101\rangle \\ & + C_{011}|011\rangle + C_{110}|110\rangle + C_{200}|200\rangle \\ & + C_{020}|020\rangle,\end{aligned} \tag{7}$$

with probability amplitudes $C_{a_1a_2m}$. Substituting the above wave function and non-Hermitian Hamiltonian into Schrödinger equation $i\partial|\psi\rangle/\partial t = H_{\rm non}|\psi\rangle$, we get a set of dynamic equations for the probability amplitudes

$$\begin{aligned}
&i\dot{C}_{000} = \Omega_d C_{001}, \quad i\dot{C}_{001} = \Delta' C_{001} + g(C_{100} + C_{010}) + \Omega_d(\sqrt{2}C_{002} + C_{000}),\\
&i\dot{C}_{100} = (\Delta' - U/2)C_{100} + gC_{001} + \Omega_d C_{101}, \quad i\dot{C}_{010} = (\Delta' - U/2)C_{010} + gC_{001} + \Omega_d C_{011},\\
&i\dot{C}_{002} = 2\Delta' C_{002} + \sqrt{2}gC_{101} + \sqrt{2}gC_{011} + \sqrt{2}\Omega_d C_{001},\\
&i\dot{C}_{101} = 2(\Delta' - U/4)C_{101} + \sqrt{2}gC_{002} + \sqrt{2}gC_{200} + gC_{110} + \Omega_d C_{100},\\
&i\dot{C}_{011} = 2(\Delta' - U/4)C_{011} + \sqrt{2}gC_{002} + \sqrt{2}gC_{020} + gC_{110} + \Omega_d C_{010},\\
&i\dot{C}_{110} = 2(\Delta' - U)C_{110} + gC_{001} + gC_{101},\\
&i\dot{C}_{200} = 2(\Delta' - U)C_{200} + \sqrt{2}gC_{101},\\
&i\dot{C}_{020} = 2(\Delta' - U)C_{020} + \sqrt{2}gC_{011},
\end{aligned} \tag{8}$$

where we assume $\Delta_{1,2,m} = \Delta$, $\kappa_{1,2} = \gamma_m = \kappa$, $\Delta' = \Delta - i\kappa/2$, and $g_1 = g_2 = g$. Under the assumption of the weak driving field, the probability amplitude satisfies $C_{000} \simeq 1 \gg C_{001}, C_{100}, C_{010} \gg C_{002}, C_{101}, C_{011}, C_{110}, C_{200}, C_{020}$. By neglecting the higher-order term in each equation, we can easily obtain the steady-state solutions of the above equations,

$$\begin{aligned}
C_{001} &= \frac{-2\Omega_d(U - 2\Delta + i\kappa)}{A},\\
C_{002} &= -2\sqrt{2}\Omega_d^2[8Ug^2 + C(U - 2\Delta + i\kappa)]/B,
\end{aligned} \tag{9}$$

with

$$\begin{aligned}
A &= 8g^2 + (U - 2\Delta + i\kappa)(2\Delta - i\kappa),\\
B &= A[16g^2(U - 2\Delta + i\kappa) + C(2\Delta - i\kappa)],\\
C &= (2U - 2\Delta + i\kappa)(U - 4\Delta + 2i\kappa).
\end{aligned} \tag{10}$$

Combining the above steady-state analytical result with the definition of the equal-time second-order correlation function, and the fact that $C_{000} \gg C_{001}, C_{100}, C_{010} \gg C_{002}, C_{101}, C_{011}, C_{110}, C_{200}, C_{020}$ under weak driving conditions. Using the perturbation method, we approximately obtain the analytical solution of the equal-time second-order correlation function $g_m^{(2)}(0)$ as follows:

$$\begin{aligned}
g_m^{(2)}(0) &= \frac{\langle m^\dagger m^\dagger m m\rangle}{\langle m^\dagger m\rangle^2}\\
&= \frac{2|C_{002}|^2}{(|C_{001}|^2 + |C_{101}|^2 + |C_{011}|^2 + 2|C_{002}|^2)^2}\\
&\approx \frac{2|C_{002}|^2}{|C_{001}|^4}.
\end{aligned} \tag{11}$$

B. Numerical simulation

To verify the validity of the analytical results, we numerically study the quantum dynamics of the system. Considering the dissipations of microwave cavity modes and the magnon mode, the dynamical evolution of the system is described by the quantum master equation

$$\dot{\rho} = -i[H, \rho] + \frac{\kappa_1}{2}\mathcal{L}[a_1]\rho + \frac{\kappa_2}{2}\mathcal{L}[a_2]\rho + \frac{\gamma_m}{2}\mathcal{L}[m]\rho, \tag{12}$$

where $\mathcal{L}[o]\rho = 2o\rho o^\dagger - o^\dagger o\rho - \rho o^\dagger o$ is the Lindblad superoperator for the arbitrary system operator o. Here, $\hat{\rho}$ is the

density operator of the system. We are concerned with the second-order correlation function in the steady state, so we need the steady-state density operator $\hat{\rho}_s$, which can be obtained by setting $\partial\rho/\partial t = 0$. Therefore, the numerical result of the equal-time second-order correlation function is

$$g_m^{(2)}(0) = \frac{\langle m^\dagger m^\dagger m m\rangle}{\langle m^\dagger m\rangle^2} = \frac{\mathrm{Tr}(m^\dagger m^\dagger m m\rho_s)}{[\mathrm{Tr}(m^\dagger m\rho_s)]^2}. \tag{13}$$

The second-order correlation function of magnons has been used in most experimental and theoretical studies as a basis for determining the single-magnon blockade effect. Here, $g^{(2)}(0) < 1$ corresponding to the sub-Poissonian statistics, which implies a magnon antibunching effect. $g^{(2)}(0) > 1$ corresponding to the super-Poissonian statistics, which implies a magnon bunching effect.

IV. MAGNON BLOCKADE EFFECT

According to the analytical solution for the equal-time second-order correlation function, if setting $C_{002} = 0$, then $g_m^{(2)}(0) \to 0$, generating a complete magnon blockade effect. Thus, we obtain the optimal parameter conditions for the UMB

$$\begin{aligned} 0 = {} & 8g^2U + 2U^3 + 28U\Delta^2 - 14U^2\Delta \\ & - 16\Delta^3 - 7U\kappa^2 + 12\Delta\kappa^2, \end{aligned} \tag{14}$$

$$0 = 7U^2\kappa + 24\Delta^2\kappa - 28U\Delta\kappa - 2\kappa^3, \tag{15}$$

and according to Eq. (15), we are able to derive

$$\begin{aligned} \Delta_1 &= (7U - \sqrt{12\kappa^2 + 7U^2})/12, \\ \Delta_2 &= (7U + \sqrt{12\kappa^2 + 7U^2})/12, \\ U_1 &= 2\Delta + [\sqrt{2/7(1 + 2\Delta^2)}], \\ U_2 &= 2\Delta - [\sqrt{2/7(1 + 2\Delta^2)}], \end{aligned} \tag{16}$$

when g and κ are determined, the optimal parameters Δ_{opt} and U_{opt} can be obtained from Eqs. (14) and (15). Figure 2 shows the Δ_{opt} and U_{opt} as functions of g/κ. It can be noticed that the optimal parameters are valid at $g/\kappa > 0.67$. At the same time, the optimal Kerr nonlinearity U_{opt} increases [Fig. 2(a)] or decreases [Fig. 2(b)] with increasing coupling strength g/κ. This indicates that perfect magnon blockade effect can be observed in the strong or weak Kerr nonlinearity.

In order to verify the above analysis, we investigate the effect of the detuning on the antibunching characteristics of the magnon. Figure 3 displays the equal-time second-order correlation function $g_m^{(2)}(0)$ as a function of the detuning Δ/κ for different U. We find that the numerical results are in good agreement with the analytical results, which proves the validity of Eq. (11). According to Fig. 2, we know that when fixing the values of g, the optimal parameters are obtained as follows: for $g/\kappa = 0.8$, $\Delta_{\mathrm{opt}} \approx \pm 0.1\kappa$ and $\Delta_{\mathrm{opt}} \approx \pm 1.3\kappa$. It can be seen from Fig. 3 that the strongest magnon blockade occurs at the optimal detuning, and the minimum value of the corresponding $g_m^{(2)}(0)$ can reach 10^{-5}, which means that our model can obtain single-magnon sources with high purity. At the same time, we note that the numerical and analytical solutions of $g_m^{(2)}(0)$ are slightly different at the optimal

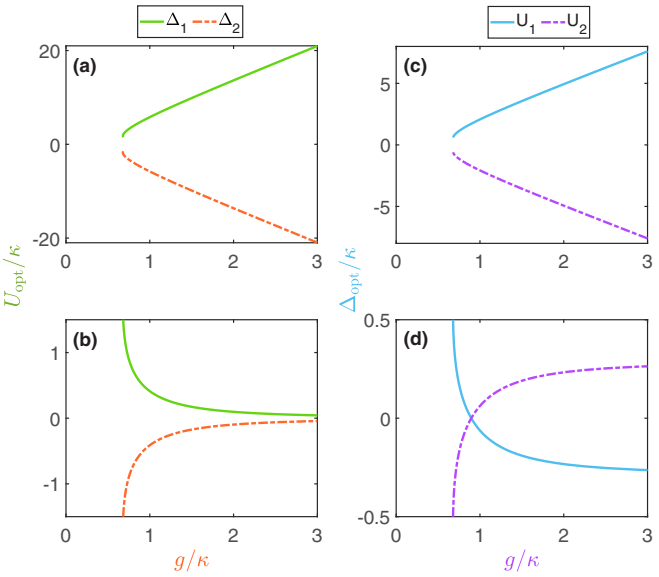

FIG. 2. The optimal detuning Δ_{opt} and Kerr nonlinearity U_{opt} vs the coupling strength g/κ.

detuning. This is due to the different Hilbert space dimensions. To obtain the analytical solutions, we omit the quantum jumps [53], and truncate the Hilbert space to two dimensions. However, in actual numerical calculations, the states $|a_1 a_2 m\rangle$ $(a_1, a_2, m > 2)$ are still occupied with small probability in order to test whether a higher number of magnon excitations can be suppressed. In Fig. 4, we plot the dynamical evolution of the equal-time second-order correlation function, which indicates the system reaches a steady state after a long evolution time. It clearly demonstrates that $g_m^{(2)}(0)$ approaches a steady value at $\kappa t \approx 15$. Based on Table I, we know that the decay

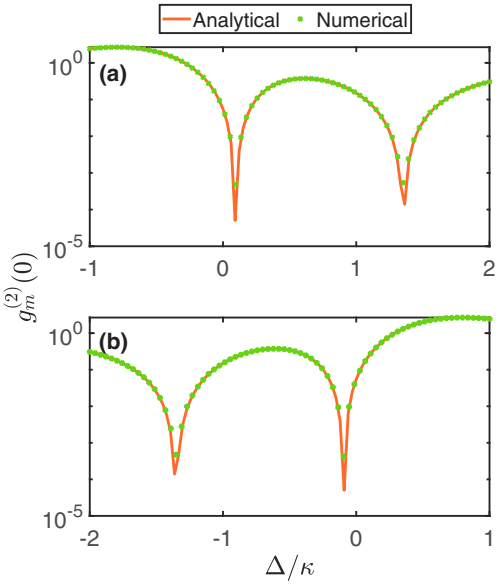

FIG. 3. The equal-time second-order correlation function $g_m^{(2)}(0)$ vs the detuning Δ/κ for different values of the Kerr nonlinearity U. (a) $U = U_1$, (b) $U = U_2$. The other parameters are $g/\kappa = 0.8$ and $\Omega_d = 0.01\kappa$.

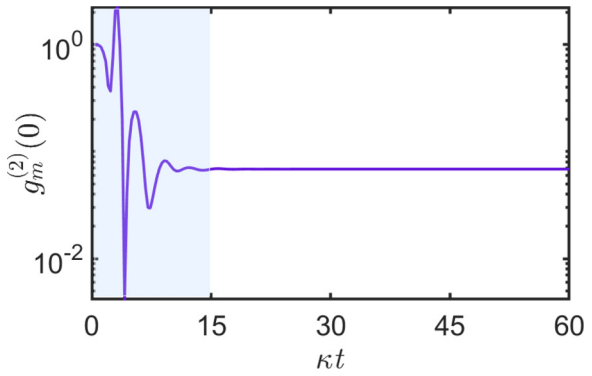

FIG. 4. The equal-time second-order correlation function $g_m^{(2)}(0)$ vs the time κt. The parameters are $g/\kappa = 0.8$, $\Delta = \Delta_{\rm opt} = 1.3\kappa$, $U = U_{\rm opt} = 3.9\kappa$, and $\Omega_d = 0.01\kappa$.

rates of both the microwave cavity mode and magnetostatic mode are $\kappa \sim$ MHz, so the corresponding relaxation time is $t \approx 15\,\mu$s.

Unconventional magnon blockade arises from the physical mechanism of the destructive quantum interference between different quantum transition pathways, as shown in Fig. 5. Obviously, there are three transition pathways corresponding to the transition from $|001\rangle$ to $|002\rangle$. The first one is the direct excitation from $|001\rangle \longrightarrow |002\rangle$, and the two magnetic dipole coupling-mediated transitions $|001\rangle \longrightarrow |100\rangle \longrightarrow |101\rangle \longrightarrow |002\rangle$ and $|001\rangle \longrightarrow |010\rangle \longrightarrow |011\rangle \longrightarrow |002\rangle$. If the Δ and U in our system satisfy the optimal conditions corresponding to the fixed value g/κ, destructive interference will occur in the three different excitation paths, the two-magnon excitation will be suppressed, and the probability of detecting the state $|002\rangle$ will be zero.

Next, we will study the influence of magnetic dipole coupling strength g on the magnon blockade effect. It is well known that if the microwave magnetic field is uniform throughout the ferromagnetic crystal, then the magnetic dipole coupling vanishes except for the Kittel mode. Thus, the coupling strength [13] between the Kittel mode and the microwave cavity mode is

$$g = \frac{\eta}{2}\gamma\sqrt{\frac{\hbar\omega\mu_0}{V}}\sqrt{2Ns}, \tag{17}$$

where ω is the resonance frequency and V is the mode volume, μ_0 is the vacuum permeability and γ is the gyromagnetic ratio, N is the total number of spins, and $s = 5/2$ is the spin number of the ground state Fe^{3+} ion in YIG. The overlapping coefficient η describes the spatial overlap between the microwave cavity and the magnon mode. Because of the high spin density of the YIG sphere and few excitations of magnons, it is easy to realize a strong coherent coupling mechanism ($g > \kappa$) through magnetic dipole interaction. We can move the position of the YIG sphere to change the magnon-photon coupling strength [54]. Thus, we can easily implement experimentally the weak and strong coupling between the magnon mode and the microwave cavity mode.

In Fig. 6, we show $g_m^{(2)}(0)$ as a function of Δ/κ for different values of g/κ. It is observed from Fig. 6 that $g_m^{(2)}(0)$ shows a strong antibunching effect at the optimal value of Δ/κ when the optimal Kerr nonlinearity $U_{\rm opt}$ is satisfied. Moreover, strong magnon blockade can be achieved both in the strong and weak coupling regimes, which provides more feasibility and flexibility for experimental implementation. In order to demonstrate the magnon blockade effect more clearly, we plot the function $\log_{10}[g_m^{(2)}(0)]$ versus the Kerr nonlinearity U/κ and the detuning Δ/κ in Fig. 7. Using Eqs. (14) and (15), we plot the optimal detuning $\Delta_{\rm opt}$ and Kerr nonlinearity $U_{\rm opt}$ versus the coupling strength g/κ, as shown in Fig. 2. [i.e., when fixing the value of g, we can get the optimal parameters as follows: for $g/\kappa = 0.8$, $\Delta_{\rm opt} \approx \pm 0.1\kappa$ ($\Delta_{\rm opt} \approx \pm 1.3\kappa$) and $U_{\rm opt} \approx \pm 0.75\kappa$ ($U_{\rm opt} \approx \pm 3.9\kappa$); for $g/\kappa = 1$, $\Delta_{\rm opt} \approx \pm 0.07\kappa$ ($\Delta_{\rm opt} \approx \pm 2.1\kappa$) and $U_{\rm opt} \approx \pm 0.37\kappa$ ($U_{\rm opt} \approx \pm 5.8\kappa$); for $g/\kappa = 2$, $\Delta_{\rm opt} \approx \pm 0.23\kappa$ ($\Delta_{\rm opt} \approx \pm 4.9\kappa$) and $U_{\rm opt} \approx \pm 0.09\kappa$ ($U_{\rm opt} \approx \pm 13.6\kappa$)]. Figure 7 shows that the values of Δ/κ and U/κ corresponding to the strongest magnon antibunching are in good agreement with the optimal value of $\Delta_{\rm opt}/\kappa$ and $U_{\rm opt}/\kappa$ derived from using Eqs. (14) and (15). On the other hand, we find that for the system without Kerr nonlinearity (i.e., $U = 0$), the second-order correlation function $g_m^{(2)}(0) \to 1$, and the system is unable to create the magnon blockade effect. Therefore,

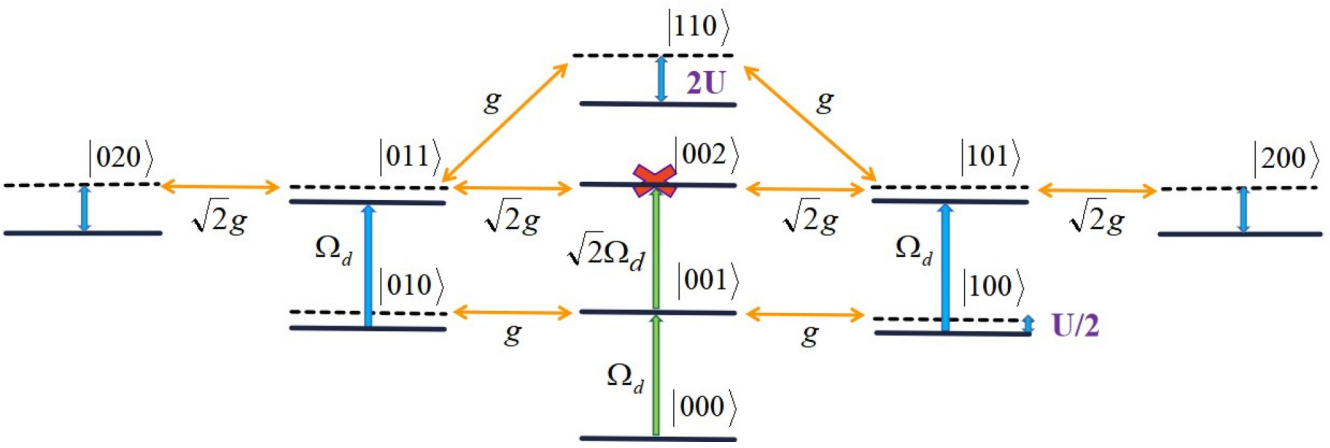

FIG. 5. Energy level diagram of the system in low-excitation subspace.

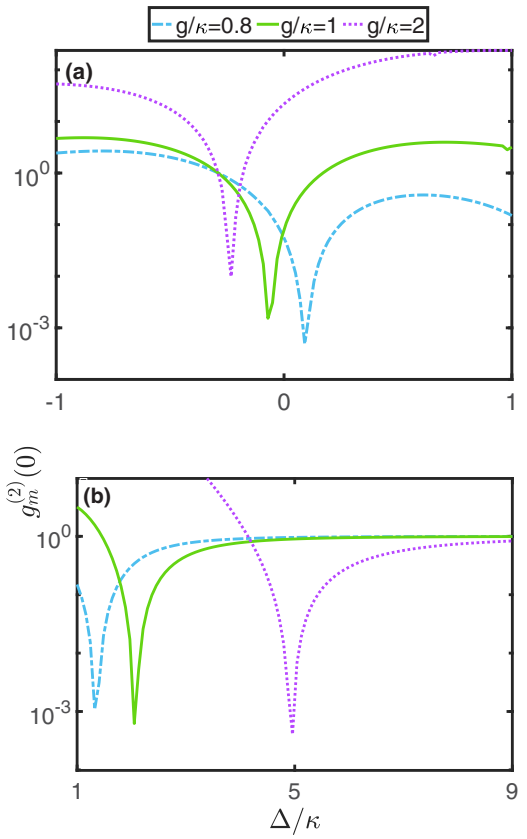

FIG. 6. The equal-time second-order correlation function $g_m^{(2)}(0)$ vs the detuning Δ/κ for different values of g/κ. The parameters are $U = U_1$ and $\Omega_d = 0.01\kappa$.

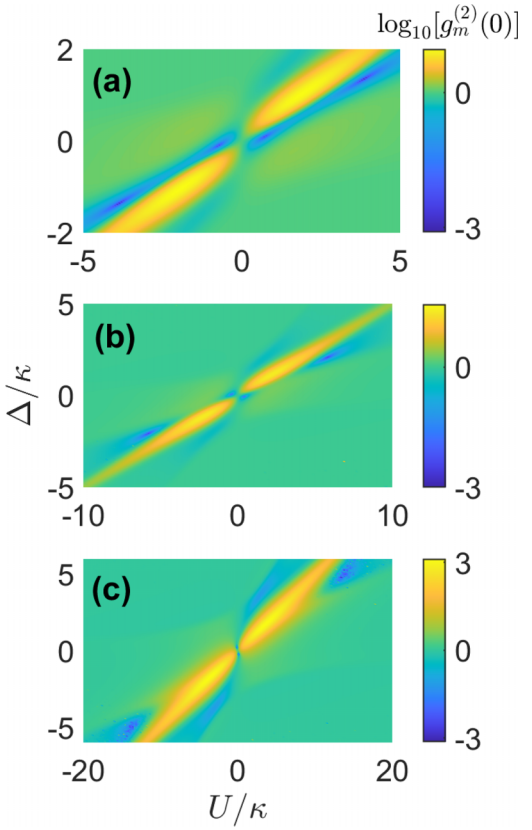

FIG. 7. Second-order correlation function on a logarithmic scale $\log_{10}[g_m^{(2)}(0)]$ as a function of U/κ and Δ/κ. Here, we chose (a) $g/\kappa = 0.8$, (b) $g/\kappa = 1$, and (c) $g/\kappa = 2$, respectively. The other parameter is taken as $\Omega_d = 0.01\kappa$.

Kerr nonlinearity is a necessary condition to achieve magnon blockade effect in our system. In the discussion above, we do not consider the effect of pure-dephasing-induced decoherences ($\gamma_p = 0$). Pure dephasing may originate from the instability of the laser drive and therefore have a perturbing effect on the magnon statistics. The effects of pure dephasing can be modeled by adding another Lindblad term of the form $\mathcal{L}[m^\dagger m]\rho = \gamma_p/2[2m^\dagger m\rho m^\dagger m - (m^\dagger m)^2\rho - \rho(m^\dagger m)^2]$ into the master equation, where γ_p is the pure dephasing rate for the magnon mode. In order to present how pure dephasing affects UMB, we plot the equal-time second-order correlation function $g_m^{(2)}(0)$ as a function of the detuning Δ/κ for different values of the pure dephasing rate γ_p, as shown in Fig. 8. We can see that with the increase of the pure-dephasing rate, $g_m^{(2)}(0)$ increases gradually at the optimal detuning ($\Delta_{\text{opt}} \approx 0.1\kappa$). For higher values of pure dephasing rates (e.g., $\gamma_p = 0.1\kappa$), $g_m^{(2)}(0)$ approaches classical Poissonian statistics. However, the magnon antibunching still exists, which indicates that the pure dephasing is not strictly required in this scheme. On the other hand, we know that the numerical results are in good agreement with the analytical results in the absence of γ_p. However, the correspondence between numerical and analytical solutions is not good when considering γ_p.

V. CONCLUSIONS

In conclusion, we have proposed a method to realize the UMB effect based on self-Kerr and cross-Kerr nonlinearities in cavity electromagnonics. Applying the quantum master equation method, we study the dynamics of the second-order correlation function to observe the statistical properties of the magnons. By minimizing the result of the equal-time second-order correlation function, we derive the optimal parameter conditions required for the UMB. The numerical calculations

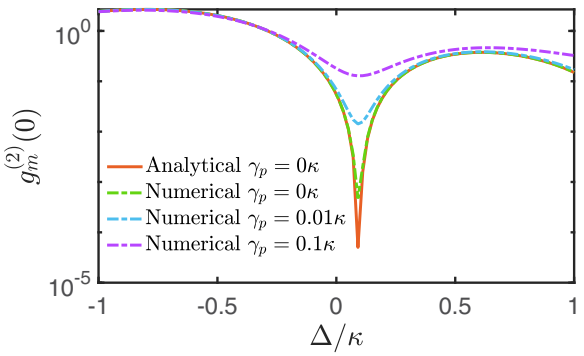

FIG. 8. The equal-time second-order correlation function $g_m^{(2)}(0)$ vs the detuning Δ/κ for different values of the pure dephasing rate γ_p. These dotted lines show the numerical results based on Eqs. (1) and (14). The green, blue, and purple dotted lines respectively represent $\gamma_p = 0\kappa$, $\gamma_p = 0.01\kappa$, and $\gamma_p = 0.1\kappa$. The yellow line indicates the analytical result based on Eq. (11). The other parameters are the same as in Fig. 3(a).

of the second-order correlation function obtained are in good agreement with the analytical calculations. We investigate the influence of Kerr nonlinearity and magnon-photon coupling strength on the MB effect. We find that the existence of Kerr nonlinearity is a crucial factor in the generation of MB. When the optimal parameter conditions are satisfied, the UMB can be generated in the strong or weak Kerr nonlinearity. At the same time, both strong and weak coupling strength are able to realize the MB effect, which enhances the feasibility of the experiment. The proposed scheme contributes to the advancement of cavity electromagnonics and offers potential applications in quantum information processing and quantum simulation.

ACKNOWLEDGMENT

This work was supported by the National Natural Science Foundation of China under Grants No. 62071412, No. 62101479, No. 12074330, and No. 12375020.

[1] Z. L. Xiang, S. Ashhab, J. Q. You, and F. Nori, Hybrid quantum circuits: Superconducting circuits interacting with other quantum systems, Rev. Mod. Phys. **85**, 623 (2013).

[2] C. L. Degen, F. Reinhard, and P. Cappellaro, Quantum sensing, Rev. Mod. Phys. **89**, 035002 (2017).

[3] A. A. Clerk, K. W. Lehnert, P. Bertet, J. R. Petta, and Y. Nakamura, Hybrid quantum systems with circuit quantum electrodynamics, Nat. Phys. **16**, 257 (2020).

[4] H. Huebl, C. W. Zollitsch, J. Lotze, F. Hocke, M. Greifenstein, A. Marx, R. Gross, and S. T. B. Goennenwein, High cooperativity in coupled microwave resonator ferrimagnetic insulator hybrids, Phys. Rev. Lett. **111**, 127003 (2013).

[5] Y. Tabuchi, S. Ishino, T. Ishikawa, R. Yamazaki, K. Usami, and Y. Nakamura, Hybridizing ferromagnetic magnons and microwave photons in the quantum limit, Phys. Rev. Lett. **113**, 083603 (2014).

[6] Y. P. Wang, J. W. Rao, Y. Yang, P. C. Xu, Y. S. Gui, B. M. Yao, J. Q. You, and C. M. Hu, Nonreciprocity and unidirectional invisibility in cavity magnonics, Phys. Rev. Lett. **123**, 127202 (2019).

[7] L. Bai, M. Harder, Y. P. Chen, X. Fan, J. Q. Xiao, and C. M. Hu, Spin pumping in electrodynamically coupled magnon-photon systems, Phys. Rev. Lett. **114**, 227201 (2015).

[8] Y. Cao, P. Yan, H. Huebl, S. T. B. Goennenwein, and G. E. W. Bauer, Exchange magnon-polaritons in microwave cavities, Phys. Rev. B **91**, 094423 (2015).

[9] X. Zhang, C. L. Zou, N. Zhu, F. Marquardt, L. Jiang, and H. X. Tang, Magnon dark modes and gradient memory, Nat. Commun. **6**, 8914 (2015).

[10] J. Xu, C. Zhong, X. Han, D. Jin, L. Jiang, and X. Zhang, Coherent gate operations in hybrid magnonics, Phys. Rev. Lett. **126**, 207202 (2021).

[11] W. Zhang, D. Y. Wang, C. H. Bai, T. Wang, S. Zhang, and H. F. Wang, Generation and transfer of squeezed states in a cavity magnomechanical system by two-tone microwave fields, Opt. Express **29**, 11773 (2021).

[12] S. Y. Guan, H. F. Wang, and X. Yi, Cooperative-effect-induced one-way steering in open cavity magnonics, npj Quantum Inf. **8**, 102 (2022).

[13] J. Li, S. Y. Zhu, and G. Agarwal, Magnon-photon-phonon entanglement in cavity magnomechanics, Phys. Rev. Lett. **121**, 203601 (2018).

[14] W. Zhang, T. Wang, X. Han, S. Zhang, and H. F. Wang, Quantum entanglement and one-way steering in a cavity magnomechanical system via a squeezed vacuum field, Opt. Express **30**, 10969 (2022).

[15] J. Cheng, Y. M. Liu, H. F. Wang, and X. Yi, Entanglement and asymmetric steering between distant magnon and mechanical modes in an optomagnonic-mechanical system, Ann. Phys. **534**, 2200315 (2022).

[16] J. Cheng, Y. M. Liu, X. Yi, and H. F. Wang, Generation and enhancement of mechanical squeezing in a hybrid cavity magnomechanical system, Ann. Phys. **534**, 2100493 (2022).

[17] J. Li, S. Y. Zhu, and G. S. Agarwal, Squeezed states of magnons and phonons in cavity magnomechanics, Phys. Rev. A **99**, 021801(R) (2019).

[18] Z. X. Liu, H. Xiong, and Y. Wu, Magnon blockade in a hybrid ferromagnet-superconductor quantum system, Phys. Rev. B **100**, 134421 (2019).

[19] L. Wang, Z. X. Yang, Y. M. Liu, C. H. Bai, D. Y. Wang, S. Zhang, and H. F. Wang, Magnon blockade in a $\mathscr{PT}$-symmetric-like cavity magnomechanical system, Ann. Phys. **532**, 2000028 (2020).

[20] Y. P. Gao, X. F. Liu, T. J. Wang, C. Cao, and C. Wang, Photon excitation and photon-blockade effects in optomagnonic microcavities, Phys. Rev. A **100**, 043831 (2019).

[21] J. K. Xie, S. L. Ma, and F. L. Li, Quantum-interference-enhanced magnon blockade in an yttrium-iron-garnet sphere coupled to superconducting circuits, Phys. Rev. A **101**, 042331 (2020).

[22] H. Xie, L. W. He, X. Shang, G. W. Lin, and X. M. Lin, Nonreciprocal photon blockade in cavity optomagnonics, Phys. Rev. A **106**, 053707 (2022).

[23] M. Moslehi, H. R. Baghshahi, M. J. Faghihi, and S. Y. Mirafzali, Photon and magnon blockade induced by optomagnonic microcavity, Eur. Phys. J. Plus **137**, 777 (2022).

[24] Y. Fang, W. Zhong, G. Cheng, and A. Chen, Magnon-photon cross-correlations via optical nonlinearity in cavity magnonical system, Opt. Express **31**, 27381 (2023).

[25] A. V. Chumak, V. I. Vasyuchka, A. A. Serga, and B. Hillebrands, Magnon spintronics, Nat. Phys. **11**, 453 (2015).

[26] X. Zhang, C. L. Zou, L. Jiang, and H. X. Tang, Strongly coupled magnons and cavity microwave photons, Phys. Rev. Lett. **113**, 156401 (2014).

[27] S. Sharma, Y. M. Blanter, and G. E. Bauer, Light scattering by magnons in whispering gallery mode cavities, Phys. Rev. B **96**, 094412 (2017).

[28] X. Zhang, N. Zhu, C. L. Zou, and H. X. Tang, Optomagnonic whispering gallery microresonators, Phys. Rev. Lett. **117**, 123605 (2016).

[29] C. H. Bai, D. Y. Wang, S. Zhang, and H. F. Wang, Qubit-assisted squeezing of mirror motion in a dissipative cavity

optomechanical system, Sci. China Phys. Mech. Astron. **62**, 970311 (2019).

[30] C. H. Bai, D. Y. Wang, S. Zhang, S. Liu, and H. F. Wang, Engineering of strong mechanical squeezing via the joint effect between Duffing nonlinearity and parametric pump driving, Photon. Res. **7**, 1229 (2019).

[31] D. Y. Wang, C. H. Bai, Y. Xing, S. Liu, S. Zhang, and H. F. Wang, Enhanced photon blockade via driving a trapped Λ-type atom in a hybrid optomechanical system, Phys. Rev. A **102**, 043705 (2020).

[32] X. Li, X. Wang, Z. Wu, W. X. Yang, and A. Chen, Tunable magnon antibunching in a hybrid ferromagnet-superconductor system with two qubits, Phys. Rev. B **104**, 224434 (2021).

[33] C. Zhao, X. Li, S. Chao, R. Peng, C. Li, and L. Zhou, Simultaneous blockade of a photon, phonon, and magnon induced by a two-level atom, Phys. Rev. A **101**, 063838 (2020).

[34] K. Wu, W. X. Zhong, G. L. Cheng, and A. X. Chen, Phase-controlled multimagnon blockade and magnon-induced tunneling in a hybrid superconducting system, Phys. Rev. A **103**, 052411 (2021).

[35] C. Kittel, On the theory of ferromagnetic resonance absorption, Phys. Rev. **73**, 155 (1948).

[36] Y. Kajiwara, K. Harii, S. Takahashi, J. I. Ohe, K. Uchida, M. Mizuguchi, and E. Saitoh, Transmission of electrical signals by spin-wave interconversion in a magnetic insulator, Nature (London) **464**, 262 (2010).

[37] L. R. Walker, Magnetostatic modes in ferromagnetic resonance, Phys. Rev. **105**, 390 (1957).

[38] P. C. Fletcher and R. O. Bell, Ferrimagnetic resonance modes in spheres, J. Appl. Phys. **30**, 687 (1959).

[39] Q. A. Turchette, C. J. Hood, W. Lange, H. Mabuchi, and H. J. Kimble, Measurement of conditional phase shifts for quantum logic, Phys. Rev. Lett. **75**, 4710 (1995).

[40] D. J. Brod and J. Combes, Passive CPHASE gate via cross-Kerr nonlinearities, Phys. Rev. Lett. **117**, 080502 (2016).

[41] M. D. Lukin and A. Imamoğlu, Nonlinear optics and quantum entanglement of ultraslow single photons, Phys. Rev. Lett. **84**, 1419 (2000).

[42] Y. B. Sheng, F. G. Deng, and H. Y. Zhou, Efficient polarization-entanglement purification based on parametric down-conversion sources with cross-Kerr nonlinearity, Phys. Rev. A **77**, 042308 (2008).

[43] F. Zou, L. B. Fan, J. F. Huang, and J. Q. Liao, Enhancement of few-photon optomechanical effects with cross-Kerr nonlinearity, Phys. Rev. A **99**, 043837 (2019).

[44] J. Q. Liao, J. F. Huang, L. Tian, L. M. Kuang, and C. P. Sun, Generalized ultrastrong optomechanical-like coupling, Phys. Rev. A **101**, 063802 (2020).

[45] Y. M. Wang, G. Q. Zhang, and W. L. You, Photon blockade with cross-Kerr nonlinearity in superconducting circuits, Laser Phys. Lett. **15**, 105201 (2018).

[46] L. J. Feng, L. Yan, and S. Q. Gong, Unconventional photon blockade induced by the self-Kerr and cross-Kerr nonlinearities, Front. Phys. **18**, 12304 (2023).

[47] M. Moslehi, H. R. Baghshahi, M. J. Faghihi, and S. Y. Mirafzali, Nonclassicality of dissipative cavity optomagnonics in the presence of Kerr nonlinearities, Phys. Scr. **98**, 025103 (2023).

[48] R. Messina, C. Holm, and K. Kremer, Strong electrostatic interactions in spherical colloidal systems, Phys. Rev. E **64**, 021405 (2001).

[49] R. Messina, C. Holm, and K. Kremer, Strong attraction between charged spheres due to metastable ionized states, Phys. Rev. Lett. **85**, 872 (2000).

[50] H. Z. Shen, Y. H. Zhou, and X. X. Yi, Tunable photon blockade in coupled semiconductor cavities, Phys. Rev. A **91**, 063808 (2015).

[51] S. Ferretti and D. Gerace, Single-photon nonlinear optics with Kerr-type nanostructured materials, Phys. Rev. B **85**, 033303 (2012).

[52] X. Zhang, C. L. Zou, L. Jiang, and H. X. Tang, Cavity magnomechanics, Sci. Adv. **2**, e1501286 (2016).

[53] F. Minganti, A. Miranowicz, R. W. Chhajlany, and F. Nori, Quantum exceptional points of non-Hermitian Hamiltonians and Liouvillians: The effects of quantum jumps, Phys. Rev. A **100**, 062131 (2019).

[54] D. Zhang, X. Q. Luo, Y. P. Wang, T. F. Li, and J. Q. You, Observation of the exceptional point in cavity magnon-polaritons, Nat. Commun. **8**, 1368 (2017).